On numerical methods for nonlinear singularly perturbed Schrödinger problems

A.I. Ávila[1], A. Meister[2], M. Steigemann[2]

[1] *CMCC, Universidad de La Frontera, Temuco, Chile*
[2] *Department of Mathematics and Natural Sciences, University of Kassel, Germany*

Abstract. Nonlinear Schrödinger equations (NSE) model several important problems in Quantum Physics and Morphogenesis. In case of singularly perturbed problems, the theory have made interesting progress, but numerical methods have not been able to come up with small values of the singular parameter ε. Moreover, the saddle-point characteristic of the associated functional is another challenge that it was first studied by Choi & McKenna, who developed the Mountain Pass Algorithm (MPA). We will focus on NSE where a uniqueness result for ground-state solutions is obtained.
In this article, we develop a new method to compute positive mountain pass solutions, which improves the results for a large range of singular parameters. We extend ideas from MPA considering the singulary perturbed problems by developing a finite element approach mixed with steepest descend directions. We use a modified line search method based on Armijo's rule for improving the Newton search and Patankar trick for preserving the positiveness of the solution. To improve the range of the singular parameter, adaptive methods based on Dual Weighted Residual method are used. Our numerical experiments are performed with the deal.II library and we show that it is possible to get solutions for $\varepsilon = 10^{-6}$ improving the current results in four order of magnitude. At this level, machine precision must be considered for further studies.

Key Words: singularly perturbed Schrödinger problems, Patankar trick, dual weighted residual method.

1. Introduction

Singularly perturbed nonlinear Schrödinger equations are very used models for understanding different physical and biological complex problems. Numerical methods have been developed to obtain more precise solutions for understanding the nonlinear effect on the phenomena. For example, in quantum mechanics particles at very low temperatures occupy the same low energy level behaving as a single large atom, the so-called *Bose-Einstein Condensation* (BEC). Experimental evidence for ^{87}Rb [AEM$^+$95], ^{23}Na [DMA$^+$95] and ^{7}Li [BSTH95] were obtained in 1995. From the Hamiltonian of the quantum field operators, Gross [Gro61] and Pitaevskii [Pit61] considered the Mean Field Theory at low temperature to derive the equation for the BEC

$$i\hbar\frac{\partial}{\partial t}\psi = \left(-\frac{\hbar^2}{2m}\Delta + \frac{m}{2}\widetilde{V} + g|\psi|^2\right)\psi.$$

Here, Δ denotes the Laplace operator. If the trapping potential $\widetilde{V}$ does not depend on time, we can consider standing wave solutions ϕ to obtain the general solution $\psi(x,t) = \phi e^{-i\mu t/\hbar}$. The condensate

In: Applied Numerical Mathematics, Volume 86 (2014), Page 22-42

ϕ is governed by the time independent nonlinear Schrödinger equation

$$\mu\phi = \left(-\frac{\hbar^2}{2m}\Delta + \frac{m}{2}\widetilde{V} + g|\phi|^2\right)\phi, \tag{1}$$

where g reflects a repulsive/attractive interaction if $g > 0$ or $g < 0$ respectively. A global minimum of the repulsive functional represents the behavior of all particles in the system. On the other hand, for attractive interactions, ground-state solutions corresponds to saddle points of changing sign functionals [KSU03], [Kav03], which will require new numerical methods.
Also, soliton solutions for nonlinear optics are ground-states from quasi-monochromatic electromagnetic wave solutions in a dieletric Kerr-type medium, which also are related with the nonlinear Schrödinger equation. See [BL03] for a detailed formulation. Finally, pattern formation modeled by (1) for $\widetilde{V}$ constant corresponds to the Turing model for morphogenesis. This phenomenon balances a time evolution with a diffusion problem related with a polynomial chemical reaction. See [NW95] for more references. The stationary solutions satisfy an equation like (1).
The main approach to compute numerical solutions is to gain a deep insight for understanding the models and their phenomena are methods related to ODE. In recent works, numerical methods involving the solution of PDE were developed for computing ground-states for BEC, [AZ07], [ZAKPG07], [ZAKPG08] and [BT03], [BD04], [BCL06], [BCW10] with quadratic potential $\widetilde{V}$, nonlinear Schrödinger systems [GRPG01], [PGL03], [RSS09], [YL08], [Yan09] and nonlinear optics [BL03]. On the other hand, for saddle points the seminal work of Choi & McKenna [CM93] develop a method based on the Mountain Pass geometry of the associated functional to (1). Also in [CZN00] a new method is described and compared with Choi & McKenna's algorithm. Based on these two results, Zhou developed a series of algorithms for computing different solutions of nonsingular problems [LZ01], [CEZ02], [WZ04], [YZ05]. The list of references presented here cannot be complete and for further information see also the cited authors' works.

The problem in calculating the BEC numerically are the very small parameters in physical applications. The atomic mass used in experiments with ^{87}Rb [AEM+95] is $m = 1.44 \times 10^{-25}$ kg and after inserting Planck's constant, $\hbar = 1.05 \cdot 10^{-34}$ J, and reordering the equation, the problem for the condensate reads

$$\left(-\varepsilon^2\Delta - V(x) + K(x)|\phi|^2\right)\phi = 0\,, \tag{2}$$

with a parameter $\varepsilon \approx 5.0 \times 10^{-8}$ and positive potentials V and K. Why this is a challenging problem, it can be seen from a result obtained by Ni & Wei in 1995 for constant potentials $V = K = 1$ on a circle domain: for sufficiently small $\varepsilon > 0$ the ground-state solution of (2) is of spike-layer type with support proportional to ε and concentrates at exactly one point x_0. This especially means that the numerical approximation scheme, for example finite elements, must detect the concentration point and a very small peak of the solution. This approach needs very efficient adaptive mesh refinement.

The focus of this work is to design efficient and robust numerical algorithms to calculate positive solutions of (3) with finite energy, especially for small values of ε. We adapt ideas from the classical Mountain Pass algorithm to solve singularly perturbed nonlinear Schrödinger equations, improving significantly previous results considering smaller perturbations ε. In section 2 we explain the theoretical framework for obtaining minimum energy solutions, called *ground-states*, and the Choi & McKenna algorithm for computing mountain pass values. We assume throughout this paper that the potentials V and K are bounded, positive C^1 smooth functions such that a positive solution exists. We develop our algorithm in section 3 based on finite elements, line searching methods for Newton schemes, Patankar trick for obtaining positive solutions, and adaptive mesh refinement. Numerical solutions of two problems are shown in section 4: one with constant potentials and the other with nonconstant

potentials proving a result of locating peaks given by [WZ97]. In the first case, we found ground-states for singular parameter as $\varepsilon = 10^{-6}$ compared with $\varepsilon = 10^{-1}$ in [Mon11], $\varepsilon = 10^{-2}$ in [CZN00] and $\varepsilon = 10^{-3}$ in [XYZ12] with Neumann boundary conditions. We notice that results for energy levels and especially estimates for the numerical error of such quantities get close to the machine precision for smaller ε posing the question how to obtain reliable results for such problems.

2. Nonlinear elliptic problems and Mountain Pass algorithm

2.1 Variational setting and ground-state solutions

In this work we consider nonlinear elliptic equations of Schrödinger type:

$$-\varepsilon^2 \Delta u(x) = f(u;x), \qquad x \in \Omega, \tag{3}$$

where $f(u;x) := -V(x)u(x) + K(x)|u(x)|^{p-1}u(x)$ and $\Omega \subset \mathbb{R}^n$ is a smooth and simple connected domain, $\varepsilon \in (0,1)$ is a (small) parameter and $1 < p < +\infty$ for $n = 2$ and $1 < p < 5$ for $n = 3$. Throughout this paper, we assume that the potentials V and K are bounded, C^1 smooth on $\mathbb{R}^n$ and

$$\inf_{x\in\mathbb{R}^n} V(x) = \overline{V} > 0, \qquad K(x) > 0\,. \tag{4}$$

We focus on positive solutions $u \geq 0$ in Ω and we prescribe homogeneous Dirichlet conditions $u = 0$ on the boundary $\partial\Omega$ assuming that particles are all located inside the domain. Let $\mathcal{E}_\varepsilon$ represent the Hilbert subspace of $H_0^1(\Omega)$ with norm

$$\|v;\mathcal{E}_\varepsilon\|^2 := \int_\Omega \left(\varepsilon^2|\nabla v|^2 + V(x)v^2\right) dx.$$

The energy functional corresponding to (3) is

$$J_\varepsilon(u) := \frac{1}{2}\int_\Omega \left(\varepsilon^2|\nabla u|^2 + V(x)u^2\right) dx - \frac{1}{p+1}\int_\Omega K(x)|u|^{p+1}\,dx. \tag{5}$$

Under conditions (4), the energy functional is continuously differentiable. It is clear that solutions to (3) correspond to critical points of J_ε, i.e.

$$J'_\varepsilon(u)(v) = 0 \qquad \text{for all} \qquad v \in \mathcal{E}_\varepsilon\,.$$

$J'_\varepsilon(u)(\,\cdot\,)$ and $J''_\varepsilon(u)(\,\cdot\,,\,\cdot\,)$ denote the derivatives of $J_\varepsilon(u)$ of order one and two, respectively. Since there is a canonical identification between a Hilbert space and its dual, we always identify the Fréchet derivative with its canonical dual. Consider the Nehari manifold

$$\mathcal{M}_\varepsilon := \left\{ v \in \mathcal{E}_\varepsilon \setminus \{0\} : \int_\Omega \left(\varepsilon^2|\nabla v|^2 + V(x)v^2\right) dx = \int_\Omega K(x)|v|^{p+1}\,dx \right\}. \tag{6}$$

Any nontrivial solution of (3) in $H_0^1(\Omega)$ belongs to (6). The ground-energy associated with a ground-state solution of (3) which minimizes J_ε on $\mathcal{M}_\varepsilon$ is defined as

$$c_\varepsilon := \inf_{v\in\mathcal{M}_\varepsilon} J_\varepsilon(v).$$

A breakthrough for the theory on the existence of solutions for such a wide class of problems as given in (3) is the nowadays classical *Mountain Pass Theorem* by Ambrosetti & Rabinowitz [AR73]. For the convenience of the reader we recall this important result. Assume that the functional $J \in C^1(\mathcal{H};\mathbb{R})$ on a Hilbert space $\mathcal{H}$ satisfies the Palais-Smale compactness condition: *each sequence* $(u_k)_{k\in\mathbb{N}} \subset \mathcal{H}$ *such that* $(J(u_k))_{k\in\mathbb{N}}$ *is bounded and* $J'(u_k) \to 0$ *in* $\mathcal{H}$*, contains a subsequence which converges in* $\mathcal{H}$*.* In addition, suppose that the topological shape of the energy functional over the underlying space $\mathcal{H}$ satisfies:

(a) $J(0) = 0$ (a low spot at zero),

(b) there exists a *ring of mountains* given by the constants $r, a > 0$ such that $J(u) \geq a$ if $\|u\|_{\mathcal{H}} = r$,

(c) there exists a *low spot* beyond the mountains given by an element $v \in \mathcal{H}$ with $\|v\|_{\mathcal{H}} > r$, $J(v) < 0$.

Let Γ be the set of all paths from the low spot at zero over the ring of mountains to the other low spot (see also the definition (8) below), then the following result guarantees the existence of a so-called *mountain pass* solution:

Theorem 1 (Mountain Pass [AR73]). *The value*

$$c := \inf_{g\in\Gamma} \max_{0\leq t\leq 1} J(g(t))$$

is a critical value of J, namely there exists $0 \neq u \in \mathcal{H}$ such that

$$J(u) = c \qquad \text{and} \qquad J'(u)(v) = 0 \quad \text{for all} \quad v \in \mathcal{H}.$$

Under assumptions (4), the ground-energy is a mountain pass value associated with J_ε in the sense [WZ97]

$$c_\varepsilon = \inf_{v\in\mathcal{M}_\varepsilon} J_\varepsilon(v) = \inf_{g\in\Gamma_\varepsilon} \max_{0\leq t\leq 1} J_\varepsilon\big(g(t)\big) = \inf_{v\in\mathcal{E}_\varepsilon\setminus\{0\}} \max_{t\geq 0} J_\varepsilon(tv) \tag{7}$$

where

$$\Gamma_\varepsilon := \big\{g \in C\big([0,1];\mathcal{E}_\varepsilon\big) : g(0) = 0, g(1) = v, J_\varepsilon(v) \leq 0\big\}. \tag{8}$$

2.2 Singularly perturbed problems

Singularly perturbed problems of type (3) were investigated by Wang & Zeng and many other authors. Besides existence and regularity results, the behavior of solutions of (3) was investigated in several works [Wan93], [NW95], [Gui96], [WZ97]. For constant potential functions $V = K = 1$ it was shown by Ni & Wei [NW95] that a ground-state for $\varepsilon \to 0$ is a spike-layer solution concentrating at exactly one point. To see the problems for numerical computations we recall Ni & Wei main results. Ground-state solutions u_ε are bounded independently of ε and the integral over powers of ground-state solutions is equivalent to ε^2. Thus, we have

$$\sup_{x\in\overline{\Omega}} u_\varepsilon(x) \leq C, \qquad\qquad m\varepsilon^2 \leq \int_\Omega u_\varepsilon(x)^3\,dx \leq M\varepsilon^2$$

where C, m, M are constants independent of ε. Moreover, ground-state solutions have spike-layer type and do not vanish to zero with $\varepsilon \to 0$:

Theorem 2 (Ni & Wei [NW95]). *There exists a constant $\overline{u} > 0$ such that if u_ε attains a local maximum at $x_0 \in \overline{\Omega}$ then $u_\varepsilon(x_0) \geq \overline{u}$. There exist constants η_0 and r_0 independent of x_0 and ε such that if $\varepsilon < \varepsilon_0$ and $B_{r_0\varepsilon}(x_0) \subset \Omega$, then $u_\varepsilon(x) \geq \eta_0$ for $x \in B_{r_0\varepsilon/2}(x_0)$.*

Also with $\varepsilon \to 0$ the height of the peak at x_0 does not shrink under some constant value and the shape of the peak will only change in the diameter. For $\varepsilon \to 0$, the peak will concentrate at one point:

Theorem 3 (Ni & Wei [NW95]). *For sufficiently small ε a ground-state solution u_ε has at most one local maximum and it is achieved at exactly one point $P_\varepsilon \in \Omega$. There holds $u_\varepsilon(\cdot + P_\varepsilon) \to 0$ in $C^1_{loc}(\Omega \setminus P_\varepsilon)$ and $\operatorname{dist}(P_\varepsilon, \partial\Omega) \to \max_{P\in\Omega} \operatorname{dist}(P, \partial\Omega)$ as $\varepsilon \to 0$.*

Moreover, the asymptotic behavior of the energy is known,

$$\inf_{v\in\mathcal{M}_\varepsilon} J_\varepsilon(v) \le \varepsilon^2\big(J(w)+\mathcal{O}(1)\big), \qquad \varepsilon\to 0, \tag{9}$$

where

$$J(w) := \frac{1}{2}\int_{\mathbb{R}^n}\left(|\nabla w|^2+w^2\right)dx - \frac{1}{p+1}\int_{\mathbb{R}^n}|w|^{p+1}\,dx$$

and w is the unique positive solution of the problem in the whole space $\mathbb{R}^n$ decaying at infinity, see [NW95] for more details. For non-constant potentials, solutions have a similar spike-layer characteristic, but the situation is more difficult. It was proven by Gui in [Gui96] for non-constant potentials V and a wide class of nonlinearities $f(u;\,\cdot\,)$ that multi-bump solutions concentrate at minima of V. For the perturbed problem (3), the concentration of solutions for $K=1$ was shown in [Wan93] and Wang & Zeng proved in [WZ97] the existence of ground-states under certain assumptions on the competition between the potentials: each one would try to attract the concentration of the ground-state to their minimum or maximum. Defining the function

$$g(x) := \frac{V(x)^{(2p+2+n-np)/(2p-2)}}{K(x)^{2/(p-1)}} \tag{10}$$

equation (3) has a positive ground-state solution for $\varepsilon\to 0$ if one of the following hypothesis holds true [WZ97]:

(a) there holds $\liminf_{|x|\to\infty} V(x) =: V_\infty = \sup_{x\in\mathbb{R}^n} V(x)$ and $\limsup_{|x|\to\infty} K(x) =: K_\infty = \inf_{x\in\mathbb{R}^n} K(x)$,

(b) there exists a point $x_0\in\mathbb{R}^n$ such that $V_\infty \ge V(x_0)$ and $K_\infty \le K(x_0)$ with one of the inequalities being strict,

(c) there exists a point $x_0\in\mathbb{R}^n$ such that $V_\infty^{(2p+2+n-np)/(2p-2)} \ge g(x_0)K_\infty^{2/(p-1)}$.

If

$$\frac{\liminf_{|x|\to\infty} V(x)^{(2p+2+n-np)/(2p-2)}}{\limsup_{|x|\to\infty} K(x)^{2/(p-1)}} \ge \inf_{x\in\mathbb{R}^n} g(x)$$

then for $\varepsilon\to 0$ equation (3) has a positive ground-state solution. Moreover, for every sequence $\{\widetilde{\varepsilon}_k\}\to 0$, there exists a subsequence $\{\varepsilon_k\}$ such that a sequence of positive ground-states $\{u_\varepsilon\}$ concentrates at a global minimum point of g. We refer to [WZ97] for a more detailed discussion. This spike-layer behavior of ground-states is a very important detail for designing numerical algorithms and good initial values required for fast convergence. Especially in situations, where concentration points are not known, efficient adaptive mesh refinement which detects the local behavior of solutions is indispensable.

2.3 Mountain Pass algorithm

An algorithm for the numerical calculation of solutions of (3) based on the Mountain Pass Theorem was suggested by Choi & McKenna. Exploiting the topological shape of the energy functional J over the underlying Hilbert space $\mathcal{H}$, the Mountain Pass algorithm (MPA) was given in [CM93]. We reword a slightly modified version from [CDN01]:

Step 1. Take an initial guess $w_0\in\mathcal{H}$ such that $w_0\neq 0$ and $J(w_0)\le 0$ (outside the ring of mountains).

Step 2. Find $t^*\in(0,1)$ such that $J(t^*w_0) = \max_{0\le t\le 1} J(tw_0)$, set $u_0 := t^*w_0$ (find the point on the edge of the ring of mountains on the straight path from zero to the initial guess)

Step 3. Calculate the direction of steepest descent: Compute $J'(u_0)$ and set $v = J'(u_0)$

Step 4. If $\|v\|_{\mathcal{H}} \leq \text{tol}$, stop, else

Step 5. Let $w = u_0 - v$ and find $t^* > 0$ such that $J(t^*w) = \max_{t>0} J(tw)$

Step 6. If $J(t^*w) < J(u_0)$, set $u_0 = t^*w$ and goto step 3, else set $v := \frac{1}{2}v$ and go to step 5

Indeed, the topological shape of the functional makes this approach very convenient for developing numerical methods. As long as $V > 0$ and $K > 0$, there holds

$$\frac{1}{2}J_{1,\varepsilon}(v) - \frac{1}{p+1}J_2(v) := \frac{1}{2}\int_\Omega \left(\varepsilon^2|\nabla v|^2 + V(x)v^2\right) dx - \frac{1}{p+1}\int_\Omega K(x)|u|^{p+1}\, dx$$

with $J_{1,\varepsilon}(\cdot) \geq 0$ and $J_2(\cdot) \geq 0$. For every fixed $v \in H_0^1(\Omega)$ the mapping

$$t \mapsto J_\varepsilon(tv) = \frac{1}{2}t^2 J_{1,\varepsilon}(v) - \frac{1}{p+1}t^{p+1}J_2(v) \tag{11}$$

has zeros at $t = 0$ and at

$$t_0 := \left(\frac{(p+1)}{2}\frac{J_{1,\varepsilon}(v)}{J_2(v)}\right)^{\frac{1}{p-1}} \quad \text{if} \quad v \not\equiv 0\,.$$

Then, the unique maximum is at $t_{\max} := J_{1,\varepsilon}(v)^{1/(p-1)}J_2(v)^{-1/(p-1)}$. Moreover, $J_\varepsilon(tv) \to -\infty$ for $t \to +\infty$. The only critical points of J_ε are either at zero or on the edge of the *ring of mountains*.

It is known that MPA of Choi & McKenna will find mainly solutions of mountain pass type with Morse index 1 or 0 [CZN00], [CDN01]. There are various modifications in the literature to obtain multiple solutions with higher Morse index, see [DCC99], [WZ04], [XYZ12] for more details.
In this work we focus on the computation of positive mountain pass solutions of (3). We combine ideas used in the MPA together with Newton's method, appropriate line searching and error control with adaptive mesh refinement. We want to remark that our assumptions on V and K guarantee the existence of a positive ground-state [WZ97], but in general a positive mountain pass solution is not unique. The computed solution will depend on the initial value and there is no guarantee that it is a ground-state.

3. Patankar-Newton scheme for Mountain Pass problems

3.1 Discretization and finite element approximation

We introduce the notation of weak solutions and the discretization of (3) into finite elements. A function $u \in H_0^1(\Omega) =: \mathcal{V}$ is called a weak solution of (3), if

$$A(u)(\varphi) := \varepsilon^2(\nabla u, \nabla\varphi)_\Omega - (f(u), \varphi)_\Omega = 0 \quad \text{for all} \quad \varphi \in \mathcal{V}. \tag{12}$$

Clearly, any weak solution $u \in \mathcal{V}$ is a critical point of the energy functional (5): $J'_\varepsilon(u)(\varphi) = A(u)(\varphi)$ for $\varphi \in \mathcal{V}$. For any measurable set M we denote the $L^2(M)$-scalar product by $(\,\cdot\,,\,\cdot\,)_M$. The discretization of the variational problem (12) seeks approximations $u_h \in \mathcal{V}_h$ in a finite dimensional subspace $\mathcal{V}_h \subset \mathcal{V}$,

$$A(u_h)(\varphi_h) = \varepsilon^2(\nabla u_h, \nabla\varphi_h)_\Omega - (f(u_h), \varphi_h)_\Omega = 0 \quad \text{for all} \quad \varphi_h \in \mathcal{V}_h. \tag{13}$$

We consider approximations with (finite element) subspaces of the form

$$\mathcal{V}_h := \left\{v \in \mathcal{V} : v\big|_{\mathcal{C}} \in P(\mathcal{C}), \mathcal{C} \in \mathcal{T}_h\right\}.$$

Here, $\mathcal{T}_h$ is a decomposition of Ω (the mesh) into quadrilaterals $\mathcal{C}$ (cells) of diameter $h_\mathcal{C}$ and $h := \max_{\mathcal{C}\in\mathcal{T}_h} h_\mathcal{C}$ is the global discretization width. The space $P(\mathcal{C})$ denotes a suitable space of polynomial-like shape functions defined on the cell $\mathcal{C} \in \mathcal{T}_h$. For example, 'bilinear' elements are obtained as usual via a *bilinear* transformation from the space of *bilinears* $Q_1\big(\widehat{\mathcal{C}}\big) = \text{span}\{1, x_1, x_2, x_1x_2\}$ on the unit cell $\widehat{\mathcal{C}} = [0,1] \times [0,1]$, see e.g. [BS02] for more technical details on finite elements. We look for solutions $u_h \in \mathcal{V}_h$ of the discrete problem (13). With a nodal basis $\{\phi_h^i, i = 1, \ldots, N\}$ of the finite element space $\mathcal{V}_h$, $\dim(\mathcal{V}_h) = N$, the discrete problem (13) can be converted to a system of algebraic equations for the vector $\boldsymbol{u} = (u_i)_{i=1}^N$ of coefficients in the decomposition $u_h = \sum_{i=1}^N u_i\phi_h^i$:

$$\varepsilon^2 \boldsymbol{A}\boldsymbol{u} - \boldsymbol{F}(\boldsymbol{u}) = \boldsymbol{0}. \tag{14}$$

The entries of the matrix $\boldsymbol{A} = (a_{ij})_{i,j=1}^N$ in (14) are given by $a_{ij} = (\nabla\phi_h^j, \nabla\phi_h^i)_\Omega$ and the vector corresponding to the nonlinearity reads

$$\big(\boldsymbol{F}(\boldsymbol{u})\big)_i = \big(f(u_h), \phi_h^i\big)_\Omega, \qquad i = 1, \ldots, N.$$

An iteration scheme for solving the nonlinear problem (12) as well as the corresponding discrete copy (13) can be formulated in general form as follows:

Step 1. *Initialization:* Compute an initial solution $u^{(0)} \in \mathcal{V}$.

Step 2. *Iteration:* Compute a new search direction d.

Step 3. *Update:* Update $u^{(j+1)} = u^{(j)} + \lambda d$, where the step length λ is chosen due to, e.g., Armijo's rule.

Step 4. *Error estimation:* Compute the residual and stop if $\big\|A\big(u^{(j+1)}\big)(\varphi)\big\| < \text{tol}$, otherwise set $j := j + 1$ and continue the iteration with step 2.

We will discuss different aspects for the choice of the search direction together with step length control. Moreover, we have to ensure that solutions are always positive. In a discrete context, this iteration scheme cannot overcome the discretization error. Using finite elements based on polynomials of fixed degree on all cells, increasing the accuracy of the approximation is always related to mesh refinement. We will accomplish this iteration scheme with a mesh refinement strategy in combination with an error control strategy.

3.2 Compute the search direction

Let us assume that we are on the edge of the ring of mountains around the low spot at zero described by the topological shape of the energy functional over the underlying space $\mathcal{V}$. Searching for a mountain pass of the functional $J_\varepsilon(\cdot)$, a search direction d should be a direction of descent:

$$J_\varepsilon'\big(u^{(j)}\big)(d) < 0 \tag{15}$$

and we call a direction *acceptable*, if (15) is fulfilled, see also [Kel99]. There are different possibilities for computing a search direction in this context. The *direction of steepest descent* used in the Mountain Pass algorithm is defined as the direction where the gradient is as negative as possible. The steepest descent direction can be computed as solution of the problem [CM93]

$$\varepsilon^2(\nabla d, \nabla\varphi)_\Omega = -J_\varepsilon'\big(u^{(j)}\big)(\varphi) \quad \text{for all} \quad \varphi \in \mathcal{V}\ . \tag{16}$$

Another possibility is Newton's direction:

$$A'\big(u^{(j)}\big)(d, \varphi) = -A\big(u^{(j)}\big)(\varphi) \quad \text{for all} \quad \varphi \in \mathcal{V}, \tag{17}$$

where the directional derivative can be computed to

$$A'(u)(\psi;\varphi) = \varepsilon^2(\nabla\psi,\nabla\varphi)_\Omega - (f'(u)\psi,\varphi)_\Omega, \qquad \varphi,\psi\in\mathcal{V}$$

and $f'(u) = -V(x) + pK(x)|u|^{p-1}$, $p>1$. Newton's method is the standard procedure for solving nonlinear problems. Providing quadratic convergence properties locally near solutions, a drawback of Newton's method is the computation of the derivative of the functional $A(\cdot)$ in every iteration step, which means that the system matrix has to be recalculated in each inner loop. It is also well-known that starting the iteration far away from a solution, convergence is very slow and the iteration may finally diverge due to the local convergence properties of the algorithm.
A short calculation shows that the direction of steepest descent is always acceptable since

$$J'_\varepsilon\big(u^{(j)}\big)(d) = -\varepsilon^2(\nabla d,\nabla d)_\Omega < 0.$$

Let us assume that $u_h^{(j)}\in\mathcal{V}_h$ is a finite element approximation in iteration step $j\geq 0$. The corresponding algebraic equations are

$$\varepsilon^2\boldsymbol{A}\boldsymbol{d} = -\big(\varepsilon^2\boldsymbol{A}\boldsymbol{u}^{(j)} - \boldsymbol{F}(\boldsymbol{u}^{(j)})\big)$$

and the discrete condition for $\boldsymbol{d}$ being an acceptable direction reads

$$\big(\varepsilon^2\boldsymbol{A}\boldsymbol{u}^{(j)} - \boldsymbol{F}(\boldsymbol{u}^{(j)})\big)\cdot\boldsymbol{d} < 0\,.$$

Since $\boldsymbol{A}$ is positive definite, we have

$$-\big(\varepsilon^2\boldsymbol{A}\boldsymbol{u}^{(j)} - \boldsymbol{F}(\boldsymbol{u}^{(j)})\big)\cdot\boldsymbol{A}^{-1}\cdot\big(\varepsilon^2\boldsymbol{A}\boldsymbol{u}^{(j)} - \boldsymbol{F}(\boldsymbol{u}^{(j)})\big) < 0 \quad \text{for all} \quad \varepsilon>0.$$

A main advantage is that the iteration using the steepest descent direction does globally converge (see e.g. [Kel99]), but unfortunately in an unpracticable slow manner. The Newton direction is not necessarily acceptable,

$$A\big(u^{(j)}\big)(d) = -A'\big(u^{(j)}\big)(d,d) = -\varepsilon^2(\nabla d,\nabla d)_\Omega + \big(f'\big(u^{(j)}\big)d,d\big)_\Omega\,.$$

The corresponding algebraic equations for the Newton direction read

$$\big(\varepsilon^2\boldsymbol{A} - \nabla\boldsymbol{F}(\boldsymbol{u}^{(j)})\big)\boldsymbol{d} = -\big(\varepsilon^2\boldsymbol{A}\boldsymbol{u}^{(j)} - \boldsymbol{F}(\boldsymbol{u}^{(j)})\big) \tag{18}$$

with the components $\big(\nabla\boldsymbol{F}(\boldsymbol{u}^{(j)})\big)_{ij} = \big(f'(u_h^{(j)})\phi_h^j,\phi_h^i\big)_\Omega$.

Remark 1: In contrast to the direction of steepest descent, Newton's direction has no direct topological interpretation. If the Newton direction d is not acceptable, we have computed a direction, where the gradient of the functional J_ε grows up. With regard to our problem we *go up* the mountain. A better choice is the opposite direction and we change the sign of d.

There are mainly two ingredients for the success of Newton's method. The first one is a good initial guess, otherwise convergence is very slow or may fail due to the local characteristic of the method. The steepest descent direction provides global convergence and it can be used in the beginning of the iteration far away from a solution, pushing the iterate closer to the region of fast convergence of the Newton scheme. In a vicinity of a solution one can switch to Newton's method, which takes into account the nonlinearity and it should converge faster. Another important tool is step length control and we will discuss it shortly in the next paragraph.
Secondly, the problem has to be non-degenerate: $J''_\varepsilon(u^{(j)})$ has to be invertible. This is a more crucial

problem. While looking for a mountain pass, solutions of this type are usually saddle points and the second derivative of the functional is singular. This problem was discussed in [WZ04] and it can be overcome using a generalized inverse. If the second derivative of the energy functional is singular, the Newton direction can be calculated as the least-norm solution of the minimization problem

$$\min_{d\in\mathcal{V}} \left\| J_\varepsilon''\big(u^{(j)}\big)(d) + J_\varepsilon'\big(u^{(j)}\big) \right\|_2 \tag{19}$$

in an adequate subspace of $\mathcal{V}$. Nevertheless, the weak problem (17) can be solved in many cases even if the second derivative is close to singular [WZ04]. In practical computations, the second derivative of the energy functional is computed at an iterate $u^{(j)}$ and the numerical approximation of the second derivative can be close to singular. The resulting algebraic equations can still be solved precisely using appropriate preconditioners. We will come back to this point when showing numerical examples.

3.3 Line searching methods

As presented in the previous section, a search direction d is acceptable, if the gradient of the functional decreases. But Newton's method only provides local convergence properties and a full iteration step does not necessarily pushes the iterate closer to a solution. A possibility to overcome this drawback is to introduce a step length $\lambda \in (0, 1]$ and define the update of the iterate to

$$u^{(j+1)} = u^{(j)} + \lambda d.$$

To determine the step length λ, a commonly used condition for nonlinear systems of equations is a discrete Armijo rule [Arm66] of the form

$$\left\| A\big(u_h^{(j)} + \lambda d_h\big)(\varphi) \right\|_2 < (1 - \alpha\lambda) \left\| A\big(u_h^{(j)}\big)(\varphi) \right\|_2$$

tracking down the residual. Looking again on the topological shape of a mountain pass, such a step length can be too large and miss the *bottom* of the mountain pass. In [Kel99] a sufficient condition for calculating λ is suggested for finding the local minimum of a functional in a local basin of the initial guess. Thereby, λ and consequently $u^{(j)} + \lambda d$ is accepted, if

$$J_\varepsilon\big(u^{(j)} + \lambda d\big) - J_\varepsilon\big(u^{(j)}\big) < \alpha\lambda J_\varepsilon'\big(u^{(j)}\big)(d) < 0 \tag{20}$$

with a positive parameter $\alpha \in (0, 1)$. While zero is a local minimum of J_ε, condition (20) does not make sense in our situation and may pull the iterate down the mountain. We employ a slightly modified version and accept a step length λ, if

$$J_\varepsilon\big(t^*(u^{(j)} + \lambda d)\big) - J_\varepsilon\big(u^{(j)}\big) < \alpha\lambda J_\varepsilon'\big(u^{(j)}\big)(d) < 0, \tag{21}$$

with the parameter t^* chosen such that

$$J_\varepsilon\big(t^*(u^{(j)} + \lambda d)\big) = \max_{t>0} J_\varepsilon\big(t(u^{(j)} + \lambda d)\big).$$

Remark that t^* can be found directly for fixed λd from the unique maximum of (11). Solutions we are looking for are located on the edge of the ring of mountains, this modification prevents the iterate from *falling down* the mountain and pushes it towards the mountain pass. Usual suggestions as presented in [Kel99] are $\alpha \approx 10^{-4}$ and this parameter is intended to make (21) as easy as possible to fulfill. The iteration will be very slow if λ is too small. A strategy of this type is known as continuous Armijo's rule [Arm66] and *pushes* especially the Newton iteration from regions where convergence is slow towards the region of quadratic convergence, where finally full steps can be used.
In particular, line searching is realized in the MPA starting with step length equal to one and reducing

it by a factor of one half in each step. We suggest a polynomial line search strategy with safeguarding, see [Kel99] for a more detailed discussion. Starting with $\lambda_0 = 1$ and $\lambda_1 = \sigma_1$, where $\sigma_1 \approx 0.5$ is a chosen parameter, we iterate until (21) is fulfilled. For $k \geq 2$, λ_k is computed as the minimum of the function

$$\zeta(\lambda) := J_\varepsilon\big(t^*(u_h^{(j)} + \lambda d_h)\big),$$

by means of an interpolation, $\zeta(\lambda) \approx p(\lambda) = \zeta(0) + c_1\lambda + c_2\lambda^2$, where

$$\begin{aligned} c_1 &= \frac{\lambda_{k-1}^2\big(\zeta(\lambda_{k-2}) - \zeta(0)\big) - \lambda_{k-2}^2\big(\zeta(\lambda_{k-1}) - \zeta(0)\big)}{\lambda_{k-1}\lambda_{k-2}(\lambda_{k-1} - \lambda_{k-2})}\,, \\ c_2 &= \frac{\lambda_{k-2}\big(\zeta(\lambda_{k-1}) - \zeta(0)\big) - \lambda_{k-1}\big(\zeta(\lambda_{k-2}) - \zeta(0)\big)}{\lambda_{k-1}\lambda_{k-2}(\lambda_{k-1} - \lambda_{k-2})}\,. \end{aligned} \tag{22}$$

The polynomial p interpolates ζ in $\zeta(0)$, $\zeta(\lambda_{k-1})$ and $\zeta(\lambda_{k-2})$. It is easily seen that the extremum is given by $\lambda_{new} = -p'(0)/p''(0) = -c_1/(2c_2)$. Thus, if $p''(0) = 2c_2 > 0$, we have reached a minimum and choose $\lambda_k = \lambda_{min}$. Otherwise, we do a safeguarding and determine

$$\lambda_k = \begin{cases} \sigma_0\lambda_{k-1}, & \text{if} \quad \lambda_{new} < \sigma_0\lambda_{k-1}, \\ \sigma_1\lambda_{k-1}, & \text{if} \quad \lambda_{new} > \sigma_1\lambda_{k-1}. \end{cases}$$

Consequently, the new step length always satisfies $\sigma_0\lambda_{k-1} < \lambda_k < \sigma_1\lambda_{k-1}$. Usual values are $\sigma_0 = 0.1$ and $\sigma_1 = 0.5$, see [Kel99]. Without safeguarding the minimum can be too close to zero and the iteration can become stuck. Otherwise, choosing large steps can lead to a non-desired behavior of the iteration, as discussed previously. Also with safeguarding the iteration can be very long, especially if the derivative of the functional is close to zero, which is the case for a mountain pass. We limit the number of cycles by $k \leq k_{\max} \approx 20$. If the line search method does not produce a valid step length after this number of steps, usually $\lambda_{20} \approx 10^{-12}$, it is an indicator that the discretization is too coarse to reproduce condition (21). In this case, we stop the iteration and refine the mesh.

3.4 How to enforce positiveness of solutions - the Patankar trick

We are interested in positive solutions of the Schrödinger equation (3). But neither the search direction computed by the Newton method nor the direction of steepest descent guarantee the positiveness of the iteration $u^{(j+1)}$, even if $u^{(j)}$ is positive. There are different possibilities to enforce constraints on solutions, for example to project the iteration $u^{(j+1)}$ to the space of positive functions. This possibility is discussed in [TT12] and the projection suggested is of the form $P(u) = u - \overline{\mathrm{co}}(u)$, where $\overline{\mathrm{co}}(u)$ is the closed convex envelope of u. See [TT12] for more details. The properties of this projection used in combination with the Mountain Pass algorithm ensure convergence to a nontrivial positive solution of (3). But the closed convex envelope of a finite element solution is difficult and expensive to compute, especially on a large number of iteration steps.
We suggest another approach. Let us assume that we have the acceptable search direction d, then we modify the update of the iterate by introducing a *weight* ω such that

$$u_{h,\omega}^{(j+1)} := u_h^{(j)} + \omega d_h\,.$$

If there is a component of the discrete iterate which is negative, $\boldsymbol{u}^{(j+1)}(i) = \boldsymbol{u}^{(j)}(i) + \boldsymbol{d}(i) < 0$, we *weight* this component by means of

$$\boldsymbol{u}_\omega^{(j+1)}(i) = \boldsymbol{u}^{(j)}(i) + \omega(i)\boldsymbol{d}(i) := \boldsymbol{u}^{(j)}(i) + \frac{\boldsymbol{u}^{(j)}(i)}{\boldsymbol{u}^{(j)}(i) - \boldsymbol{d}(i)}\boldsymbol{d}(i) \tag{23}$$

for indices $i = 1, \dots, N$. If $\boldsymbol{u}^{(j)}(i) + \boldsymbol{d}(i) < 0$ the weighted component $\boldsymbol{u}_\omega^{(j+1)}(i)$ is always positive if the component $\boldsymbol{u}^{(j)}(i)$ of the previous iteration is positive:

$$\boldsymbol{u}^{(j)}(i) + \omega(i)\boldsymbol{d}(i) = \frac{\boldsymbol{u}^{(j)}(i)\boldsymbol{u}^{(j)}(i)}{\boldsymbol{u}^{(j)}(i) - \boldsymbol{d}(i)}\,.$$

Modifications of type (23) are known as Patankar trick or Patankar scheme introduced in [Pat80] and used in a specific modification to enforce conservativity, for example in [BDM03].
If the search direction d_h tends to zero, (23) clearly shows, that also the weighted direction ωd_h tends to zero and Newton's method has found a solution, if ωd_h vanishes. But the Patankar modification cannot guarantee that the weighted vector $\boldsymbol{d}_\omega$ is a direction of descent, even if the direction $\boldsymbol{d}$ satisfies this constraint. The estimate

$$0 < \frac{\boldsymbol{u}^{(j)}(i)}{\boldsymbol{u}^{(j)}(i) - \boldsymbol{d}(i)} < \frac{1}{2}$$

provides an upper bound for the weights, but negative components of $\boldsymbol{d}$ can be weighted with such a small factor that the resulting vector does not fulfill the descent condition (15). In combination with a type of line searching, this can be overcome. If the weighted direction $\boldsymbol{d}_\omega$ is not a descent direction, the Patankar trick scales the components of $\boldsymbol{d}$ down and reduces the possibility that the weighted vector loses the descent property. If we introduce a step length $\eta \in (0, 1]$ in the weighted direction,

$$\boldsymbol{d}_{\omega,\eta}(i) = \frac{\boldsymbol{u}^{(j)}(i)}{\boldsymbol{u}^{(j)}(i) - \eta\boldsymbol{d}(i)}\eta\boldsymbol{d}(i)\,,$$

the number of weighted components decreases with $\eta \to 0$ and there exist a step length η, such that the resulting weighted vector $\boldsymbol{d}_\omega$ is a descent direction. In practice, this can be realized with a simple loop, starting with $\eta_0 = 1$ and reducing the step length by a factor not too small, for example $\eta_{k+1} = 0.75\eta_k$ for $k \geq 0$. Doing line searching as described in the previous section, it guarantees condition (21) for the new iterate. The weighted i-th component now reads

$$\boldsymbol{u}_\omega^{(j+1)}(i) == \frac{\left(\boldsymbol{u}^{(j)}(i)\right)^2 - (1-\lambda)\eta\boldsymbol{u}^{(j)}(i)\boldsymbol{d}(i)}{\boldsymbol{u}^{(j)}(i) - \eta\boldsymbol{d}(i)} \tag{24}$$

and due to $-\eta\boldsymbol{d}(i) > 0$ one can directly conclude the positivity of $\boldsymbol{u}_\omega^{(j+1)}(i)$ for $\eta, \lambda \in (0, 1]$. In practice, the step length η and also the new search direction $\boldsymbol{d}_\omega$ can be very small, as we see from (24). The convergence can become very slow especially in regions far away from a solution. In such a case, one should interrupt the loop and refine the mesh. If the change in the functional value is too small, a good choice is $\varepsilon \cdot 10^{-10}$. In summary, we have proved the following result:

Lemma 4. *Starting with a positive initial solution $u^{(0)} > 0$, the modified search direction ωd_h defined component-by-component in* (23) *ensures the positiveness of the iteration $u_{h,\omega}^{(j+1)}$ for $j \geq 0$. In combination with step length control and a line searching method as given in* (24)*, the iterate $u_{h,\omega}^{(j+1)}$ fulfills the descent condition* (21)*.*

3.5 Error control and adaptive mesh refinement

Mesh refinement is one of the main keys to achieve efficient and accurate finite element schemes, especially for the Schrödinger problem (3). We know *a priori* that we compute spike-layer solutions, but we do not know the exact location and diameter of the peak. In recent works, e.g. [Mon11], [XYZ12], mesh refinement was done by hand calculating test problems, where the location of peaks where known, what in general is of course not the case. For more complex problems, an efficient mesh refinement

strategy is indispensable for obtaining reliable and accurate results.
Accuracy is always coupled with error measurement, for example, the residual

$$\left\|A\big(u_h^{(j)}\big)(\varphi_h)\right\|_2, \qquad u_h^{(j)}, \varphi_h \in \mathcal{V}_h.$$

Obviously, the residual does not provide a direct information how to adapt the mesh to improve accuracy. The iteration scheme tracks down the error to some tolerance, but cannot overcome the discretization error of the finite element approximation. Due to the very local behavior of solutions, global mesh refinement is not a realistic option, since it yields an astronomically high computational effort to obtain suitable accuracy. Thus, we take into account a different aspect of solutions of (3). We are interested in the computation of positive mountain pass solutions with finite energy. In order to calculate the energy level precisely, it is reasonable to adapt the mesh in such a way, that the error

$$E(u_h) = |J_\varepsilon(u) - J_\varepsilon(u_h)| \tag{25}$$

gets smaller with continuing the mesh refinement. An approach realizing such a strategy was developed mainly by Rannacher and co-workers, called the *dual weighted residual* (DWR) method, see e.g. [BR03] and the literature cited there. The principle idea is the following: let $J(\cdot)$ be the error functional we are interested in and (25) the error we want to control, where u is a weak or even strong solution of (3) and u_h is a finite element approximation. Introduce a *dual* variable $z \in \mathcal{V}$ as a weak solution of the variational problem

$$J'(u)(\varphi) - A'(u)(\varphi, z) = 0 \quad \text{for all} \quad \varphi \in \mathcal{V}.$$

Consequently, the discrete dual problem reads

$$J'(u_h)(\varphi_h) - A'(u_h)(\varphi_h, z_h) = 0 \quad \text{for all} \quad \varphi_h \in \mathcal{V}_h.$$

As shown in [BR03], the error (25) can be computed by

$$J(u) - J(u_h) = \rho(u_h)(z - \varphi_h) + \boldsymbol{R}_h^{(2)} \tag{26}$$

for any $\varphi_h \in V_h$ with the residual

$$\rho(u_h)(\cdot) := -A(u_h)(\cdot)\,.$$

The remainder term $\boldsymbol{R}_h^{(2)}$ is quadratic in the *primal* error $e = u - u_h$:

$$\boldsymbol{R}_h^{(2)} = \int_0^1 \Big\{ A''(u_s)(e,e,z) - J''(u_s)(e,e) \Big\} s\, ds$$

where $u_s := u_h + se$. Relation (26) provides the possibility to compute the functional error from the finite element solution and, in addition, to construct a cell-wise error indicator used for mesh refinement. Neglecting the remainder term and integration by parts yields

$$\begin{aligned} J_\varepsilon(u) - J_\varepsilon(u_h) &= \rho(u_h)(z - \psi_h) + \ldots = -A(u_h)(z - \psi_h) + \ldots \\ &= -\varepsilon^2 \big(\nabla u_h, \nabla(z - \psi_h)\big)_\Omega + \big(f(u_h), z - \psi_h\big)_\Omega + \ldots \\ &= \sum_{\mathcal{C} \in \mathcal{T}_h} \left\{ \big(\varepsilon^2 \Delta u_h + f(u_h), z - \psi_h\big)_{\mathcal{C}} + \varepsilon^2 \Big(\frac{1}{2}\big[\partial_\nu u_h\big], z - \psi_h\Big)_{\partial\mathcal{C}\setminus\partial\Omega} \right\} + \ldots, \end{aligned}$$

where $\partial_\nu u(x) := \nabla u(x) \cdot \nu(x)$ denotes the derivative in the direction of the outward normal on the cell boundary $\partial\mathcal{C}$ and $\big[\partial_\nu u\big]$ is its jump over the inter-element boundaries. The error of the functional

can be presented in terms of the cell and edge residuals of the solution weighted by the dual solution. With $\psi_h = I_h z$, where $I_h z$ denotes the nodal interpolant of the continuous function z, we have

$$E(u_h) \leq \sum_{\mathcal{C}\in\mathcal{T}_h} \Big\{ \big\|\varepsilon^2 \Delta u_h + f(u_h); L^2(\mathcal{C})\big\| \big\| z - I_h z; L^2(\mathcal{C})\big\| + \frac{\varepsilon^2}{2} \big\|\partial_\nu u_h; L^2(\partial\mathcal{C}\setminus\partial\Omega)\big\| \big\| z - I_h z; L^2(\partial\mathcal{C}\setminus\partial\Omega)\big\| \Big\} + \dots . \quad (27)$$

The dual solution z has to be computed numerically also, but with higher order than u_h, because otherwise the error would be zero. It is worth mentioning that this fact implies a necessary but even usually considerably amount of computational effort. Nevertheless, beside the Patankar-Newton approach, this strategy represents the main key for the success of the whole numerical scheme and enables the calculation of test cases with a small parameter $\varepsilon = 10^{-6}$ for the first time.

3.6 Algorithm

For the sake of completeness, we summarize the specific steps into the following algorithm. Starting from an initial coarse grid $\mathcal{T}_0$, let $\mathcal{T}_0 \subset \mathcal{T}_1 \subset \ldots \subset \mathcal{T}_l$ be a hierarchy of refined meshes with corresponding finite element spaces $\mathcal{V}_l$.

Step 1. *Initialization:* Take an initial guess $w_0 \in \mathcal{V}_0$ such that $w_0 \neq 0$ and $J_\varepsilon(w_0) < 0$. Compute $t^* = \big(J_{1,\varepsilon}(w_0)/J_2(w_0)\big)^{1/(p-1)}$ fulfilling $J_\varepsilon(t^* w_0) = \max_{t>0} J_\varepsilon(t w_0)$, set the initial solution to $u_0 := t^* w_0 \in \mathcal{V}_0$.

Step 2. *Iteration (mesh refinement):* For $l \geq 0$ do:

Step 3. *Newton iteration:* Start with $u_l^{(0)} = u_l \in \mathcal{V}_l$, for $j \geq 0$ do:

Step 4. *Compute residual:* Stop and go to step 9, if

$$\big\|A\big(u_l^{(j)}\big)\big(\varphi_l\big)\big\|_2 < tol \approx \varepsilon \cdot 10^{-10}$$

Step 5. *Search direction:* For the iterate $u_l^{(j)} \in \mathcal{V}_l$ compute the Newton direction

$$A'\big(u_l^{(j)}\big)\big(d_l^{(j)}, \varphi_l\big) = -A\big(u_l^{(j)}\big)(\varphi_l) \quad \text{for all} \quad \varphi_l \in \mathcal{V}_l$$

Step 6. Accept $d_l^{(j)}$, if $A\big(u_l^{(j)}\big)\big(d_l^{(j)}\big) < 0$, otherwise change the sign

Step 7. *Patankar trick:* Set $\eta_0 := 1$, for $k \geq 0$ do: Compute modified direction $\omega d_{l,\eta_k}$ with components

$$\boldsymbol{d}_{\omega,\eta_k}(i) := \frac{\boldsymbol{u}^{(j)}(i)}{\boldsymbol{u}^{(j)}(i) - \eta_k \boldsymbol{d}(i)} \eta_k \boldsymbol{d}(i)\,,$$

if $\omega d_{l,\eta_k}$ is a direction of descent, set $d_l^{(j)} := \omega d_{l,\eta_k}$ and go to step 8, otherwise set $\eta_{k+1} := 0.75 \cdot \eta_k$.

Step 8. *Line search:* Choose $\alpha \approx 10^{-4}$, $\sigma_0 \approx 0.1$, $\sigma_1 \approx= 0.5$.
Set $\lambda_0 = 1$ and $\lambda_1 = \sigma_1$. For $k \geq 0$ do: If $k \geq 2$ calculate the coefficients c_1 and c_2 according to (22). If $c_2 > 0$, choose $\lambda_k = -c_1/2c_2$, otherwise $\lambda_k \in [\sigma_0\lambda_{k-1}, \sigma_1\lambda_{k-1}]$. Let $w = u_l^{(j)} + \lambda_k d_l^{(j)}$ and compute $t^* = \big(J_{1,\varepsilon}(w)/J_2(w)\big)^{1/(p-1)}$ such that $J_\varepsilon(t^* w) = \max_{t>0} J(tw)$. If

$$J_\varepsilon\big(t^* w\big) - J_\varepsilon\big(u_l^{(j)}\big) < \alpha\lambda_k A\big(u_l^{(j)}\big)\big(d_l^{(j)}\big)$$

set $u_l^{(j+1)} = t^* w$, $j = j+1$ and go to step 5, otherwise set $k = k+1$.

Step 9. *Error estimation:* Evaluate a bound for the error $E(u_l)$ of the functional value using (27). If $E(u_l) < tol$, stop, otherwise refine the mesh $\mathcal{T}_l \subset \mathcal{T}_{l+1}$, interpolate $u_l \to u_{l+1} \in \mathcal{T}_{l+1}$, set $l := l + 1$ and go to step 2.

4. Numerical results

Before we show numerical results, we give some short remarks on the implementation. For numerical computations, we use the deal.II package, a C++ finite element open source library which provides data structures and algorithms needed in finite element calculations, see [BHK07] and www.dealii.org. Computations in deal.II are parallel over nodes based on MPI and built on the p4est library, see [BBHK11] and www.p4est.org. For our computations we use BiCGstab from the parallel PETSc package with the approximate inverse preconditioner ParaSails from the HyPre package, which can handle indefinite linear systems. In this first approach, we approximate solutions u_ε with biquadratic Q_2 Lagrange elements and dual solutions z with bicubic Q_3 Lagrange elements on quadrilaterals. All results were obtained on a machine with a single quad-core processor running 4 MPI processes.

Remark: As discussed in a previous paragraph, we are looking for a mountain pass where the second derivative of the functional can be zero and the solution can be a saddle point of the functional. For the discrete iteration scheme, this means that the system matrix of the Newton scheme can become not only indefinite, but also *very close* to singular. Using the BiCGstab method together with the ParaSails preconditioner designed for handling indefinite problems, we never encountered any problems solving the algebraic linear systems, even we observed that the system matrix becomes indefinite.

4.1 Example 1: Constant potentials

Utilizing $V = K \equiv 1$ and $p = 3$, we obtain an example which can be found in [NW95] and the literature therein:

$$-\varepsilon^2 \Delta u + u = u^3, \qquad u \geq 0 \quad \text{in} \quad \Omega, \qquad u = 0 \quad \text{on} \quad \partial\Omega. \tag{28}$$

From the statements in section 2.2 the shape of solutions and also the asymptotic behavior of the ground-energy are known and problem (28) is excellent to test numerical methods. Choosing the unit circle in the plane $\mathbb{R}^2$, $\Omega := \{x \in \mathbb{R}^2 : \|x\| < 1\}$, the unique ground-state solution concentrate at the origin. The spike-layer form suggests an initial guess of the following type:

$$w_0(x) := \begin{cases} c \exp\left(-\frac{\|x-x_c\|}{R-\|x-x_c\|}\right), & \text{if} \quad \|x - x_c\| < R, \\ 0, & \text{otherwise.} \end{cases} \tag{29}$$

The concentration point is the origin, $x_c = (0,0)^\top$, and depending on ε good choices for R are between 0.5 and 0.05, whereas $c = 10$ was always sufficient in our computations. We limit the number of Newton iterations to $j_{\max} \leq 4$ but run $l_{\max} = 16$ mesh refinement cycles. We stop Newton iteration and refine the mesh if $\left\|A(u_l^{(j)})\right\|_2 < tol = \varepsilon \cdot 10^{-10}$. Mesh refinement is based on the error estimator shown in section 3 and we refine 10% of the cells per cycle. The refinement algorithms in the deal.II library will flag some additional cells for smoothing the triangulation and the effective ratio of refined cells will about $20 - 30\%$. Thereby, we also allow the library to coarsen 0.1% of the cells.
Table 1 shows the numerical results obtained by the Newton iteration combined with the Patankar modification and adaptive mesh refinement. Besides the value ε the number of cells and degrees of freedom (DoF) of the finally obtained mesh are shown. The column $\|A(u_h)\|_2$ shows the residual of the final solution and $J_\varepsilon(u_h)$ is the energy value obtained. The estimated error is shown in column $E(u_h) = |J_\varepsilon(u) - J_\varepsilon(u_h)|$ and minimal as well as maximal values of u_h are given in the last two columns.

Here, we run 16 mesh refinement cycles. We want to underline, that the energy values are in absolute agreement with the asymptotically expected ones shown in (9):

$$J_\varepsilon(u_\varepsilon) = \mathcal{O}\left(\varepsilon^2\right).$$

Also the maximum of the solutions shown in the last column stay very close to a constant for $\varepsilon \to 0$ and do not fall to zero. Numerical tests suggest parameters for line search $\alpha = 10^{-4}$, $\sigma_0 = 0.1$ and $\sigma_1 = 0.5$. The limit $k_{\max} = 20$ for line search and the Patankar line search iteration is a good choice in practice. This high number of iterations gives the line search *a bit more time*, which is needed especially for small values of ε. More accuracy achieved by an iteration step here is much cheaper than refining the mesh. We choose $\beta = 0.75$ in the Patankar line search iteration. Unfortunately, for $\varepsilon = 10^{-5}$ and $\varepsilon = 10^{-6}$, Table 1 shows a loss of accuracy and especially the ground-energy is not as we expect it. All other ground-energy values shown in the table are precise up to four digits. The spike-layer solution has a very small peak and we need more mesh refinement to resolve this. Using 18 mesh refinement cycles for $\varepsilon = 10^{-5}$ and 20 cycles for $\varepsilon = 10^{-6}$ produces the results in Table 2 which are in absolute agreement with the expected asymptotic behavior. But we have to remark that residuals and error estimation are in the range of machine precision, which is around 10^{-16} for doubles in C++ on a 64bit system. From this point of view, it does not make sense to go much smaller with values for ε. In comparison to the results shown in [Mon11] for $\varepsilon \geq 10^{-1}$ and also in [CZN00] for $\varepsilon \geq 10^{-2}$, the mesh refinement strategy in combination with the positivity preserving Patankar ansatz allows for much more accurate results. As we see from the results, we need heavy refinement to resolve the peak, but using for example global mesh refinement costs would be more than 70% higher per step and would lead to astronomically large systems of nonlinear equations.
The most interesting cases are $\varepsilon = 10^{-5}$ and $\varepsilon = 10^{-6}$. Figure 1 shows the initial mesh with 5185 DoF and the mesh after 20 refinement cycles with 796657 DoF for $\varepsilon = 10^{-6}$ is shown in figure 2. In some distance from the peak of the solution at the origin near the outer boundary the strategy coarsen the mesh and refinement is only near the peak, exactly as aspected. Looking very close to the peak, shown in Figure 3 - 5, we see the very fine mesh structure around the peak and the final mesh width directly around the origin is $h = 7 \cdot 10^{-8}$. Note the plot scale! The solution is plotted around the origin in Figure 6 with the same scaling as the mesh in Figure 5. These pictures clearly show the functioning and the efficiency of the error based mesh refinement strategy.

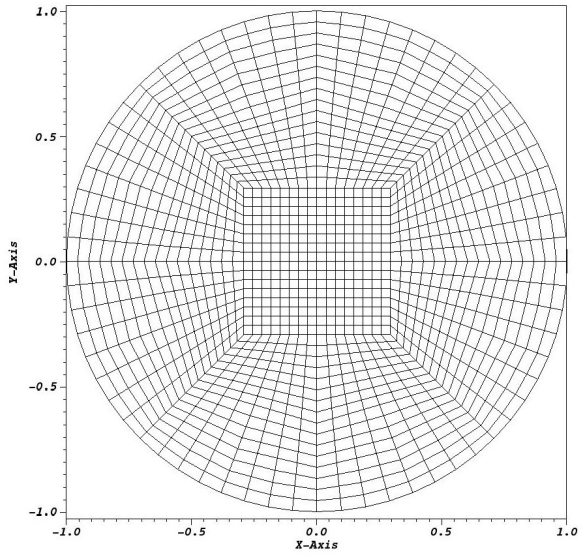

Figure 1: Example 1: Initial mesh, 5185 DoF

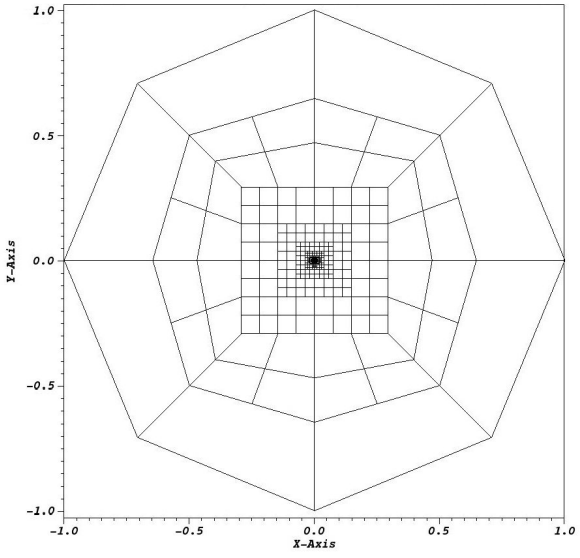

Figure 2: Example 1: Final mesh, 796657 DoF

ε	# cells	# DoF	$\|A(u_h)\|_2$	$J_\varepsilon(u_h)$	$E(u_h)$	$\min(u_h)$	$\max(u_h)$
$8.00e-01$	75122	309529	$3.33e-13$	$6.9540e+00$	$5.63e-09$	0.00	3.3333
$4.00e-01$	70598	290585	$1.79e-13$	$1.0072e+00$	$1.78e-09$	0.00	2.3444
$2.00e-01$	67892	274381	$3.56e-14$	$2.3415e-01$	$7.05e-10$	0.00	2.2073
$1.00e-01$	65726	266313	$9.90e-15$	$5.8504e-02$	$2.08e-10$	0.00	2.2062
$5.00e-02$	66815	270905	$1.06e-15$	$1.4626e-02$	$4.67e-11$	0.00	2.2062
$1.00e-02$	64703	263509	$4.97e-17$	$5.8504e-04$	$2.16e-12$	0.00	2.2062
$5.00e-03$	57794	234925	$5.32e-16$	$1.4626e-04$	$6.39e-13$	0.00	2.2062
$1.00e-03$	75395	309991	$8.71e-13$	$5.8504e-06$	$1.99e-14$	0.00	2.2062
$5.00e-04$	74360	306093	$1.40e-14$	$1.4626e-06$	$5.46e-15$	0.00	2.2062
$1.00e-04$	70793	294517	$1.50e-15$	$5.8504e-08$	$3.28e-16$	0.00	2.2062
$5.00e-05$	68294	285849	$5.59e-14$	$1.4626e-08$	$1.96e-16$	0.00	2.2062
$1.00e-05$	77369	336201	$6.32e-15$	$5.8504e-10$	$4.12e-15$	0.00	2.2062
$1.00e-06$	68132	309913	$3.56e-14$	$6.0235e-12$	$6.60e-13$	0.00	2.2091

Table 1: Example 1: Results on the unit circle, 16 refinement cycles, $V = K \equiv 1$, $p = 3$

ε	# cells	# DoF	$\|A(u_h)\|_2$	$J_\varepsilon(u_h)$	$E(u_h)$	$\min(u_h)$	$\max(u_h)$
$1.00e-05$	129227	544913	$1.89e-16$	$5.8504e-10$	$1.55e-17$	0.00	2.2062
$1.00e-06$	185999	796657	$1.12e-20$	$5.8504e-12$	$6.18e-18$	0.00	2.2062

Table 2: Example 1: Results on the unit circle after 18 and 20 cycles, $V = K \equiv 1$, $p = 3$

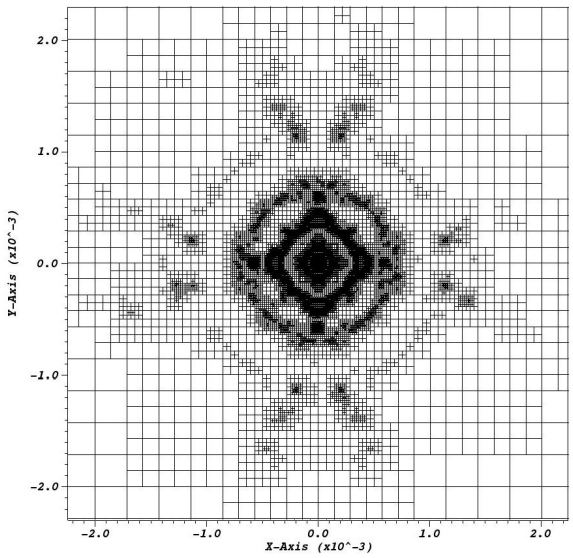

Figure 3: Example 1: Final mesh, zoom 1

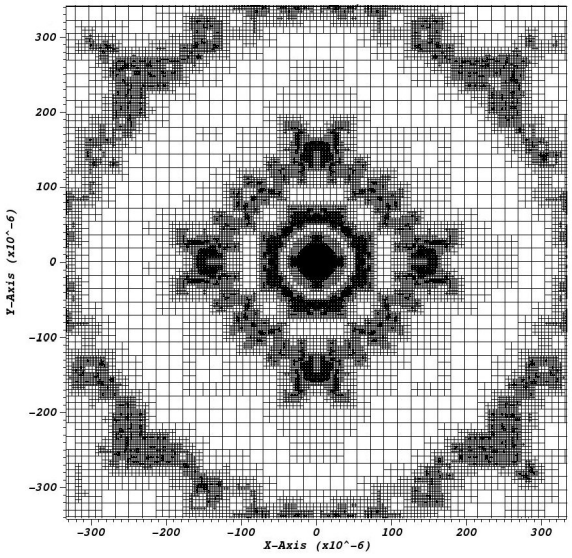

Figure 4: Example 1: Final mesh, zoom 2

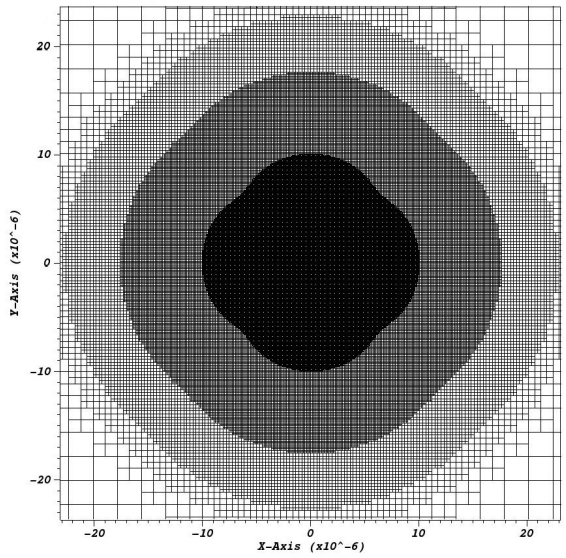

Figure 5: Example 1: Final mesh, zoom 3

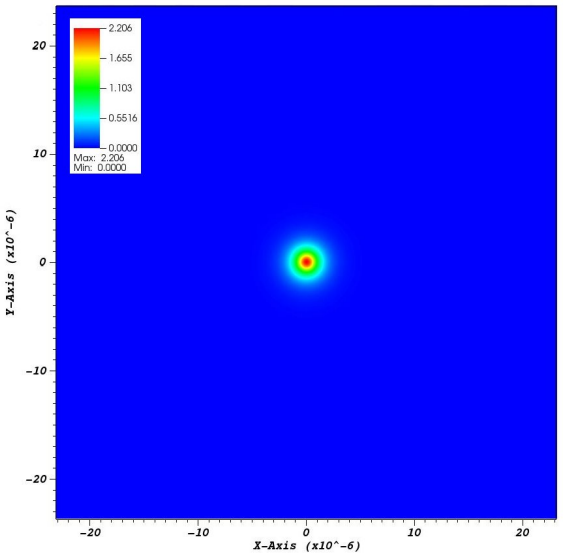

Figure 6: Example 1: Solution u, zoom 3

Another interesting question is concerned with the need for the Patankar trick in practical calculations. For $\varepsilon \geq 10^{-1}$, we observed that starting with a positive solution the iterate remains to be positive and the iteration automatically finds a positive solution also without the Patankar modification. However, for smaller values of ε, the Newton scheme destroys positiveness of the iterate in our computations and we have to apply the Patankar approach in nearly all iteration steps, which is clearly a signal, that the Patankar trick is one of the keys for computing positive solutions for small ε.

4.2 Example 2: Nonconstant potentials - on the unit circle

As a first example for nonconstant potentials we choose

$$V(x) = 1 - \frac{c}{\|x - x_0\|_2 + 1}, \qquad K(x) = \frac{1}{\|x - x_1\|_2 + 1}$$

where $c = 0.95$ is determined such that the function V has no zeros. The point $x_0 = (0,0)^\top$ is a valley of V and $x_1 = (0.5, 0.5)^\top$ is a peak of K. Table 3 shows the computed results with 16 mesh refinement cycles for $\varepsilon \geq 10^{-4}$, and 18 and 20 cycles for $\varepsilon = 10^{-5}$ and $\varepsilon = 10^{-6}$, respectively. We see the same behavior of the ground-energy as for constant potential functions: the ground-energy decreases proportional to ε^2. An interesting phenomena for this type of potentials is the concentration point of solutions. We start all calculations with the initial function w_0 given in (29), choosing $R = 0.5$, $c = 10$ and $x_0 = (0,0)^\top$. For $\varepsilon < 10^{-2}$ we adapt the diameter of the peak to $R = 0.05$. After 16 mesh refinement cycles the solution for $\varepsilon = 0.8$ is plotted in Figure 7. The concentration point is not at the minimum of the function g from (10), which is the origin. As we can see from the solution for $\varepsilon = 10^{-6}$ in Figure 8, the peak has *moved* closer to the origin. But this is in absolute agreement with the theoretical results shown in [WZ97]: the ground-state solution concentrates at the origin *only* for $\varepsilon \to 0$ and this is what we observe here. Of course, we do not have a criterion to prove, that we have calculated a ground-state. It is clear that a solution computed by Newton's method depends on the initial value. Maybe there is an initial value which produces another sequence of iterates with smaller ground-energy. The conclusion we can draw is, that we have computed a solution u_h and the corresponding numerical energy value $J_\varepsilon(u_h)$ is precise up to an error $E(u_h)$.

ε	# cells	# DoF	$\|A(u_h)\|_2$	$J_\varepsilon(u_h)$	$E(u_h)$	$\min(u_h)$	$\max(u_h)$
$8.00e-01$	70160	289979	$7.65e-13$	$8.5483e+00$	$8.89e-09$	0.00	3.8960
$4.00e-01$	80990	334905	$1.96e-13$	$7.4965e-01$	$7.96e-10$	0.00	2.2315
$2.00e-01$	70946	289861	$4.36e-14$	$1.0398e-01$	$2.85e-10$	0.00	1.5966
$1.00e-01$	66587	268793	$1.19e-14$	$1.8836e-02$	$7.33e-11$	0.00	1.3603
$1.00e-02$	65729	266981	$8.62e-17$	$7.7441e-05$	$3.34e-13$	0.00	0.8459
$1.00e-03$	46673	190345	$7.46e-19$	$5.3585e-07$	$3.89e-15$	0.00	0.6758
$1.00e-04$	86816	353543	$1.11e-17$	$5.0321e-09$	$1.03e-17$	0.00	0.6479
$1.00e-05$	111419	461961	$4.03e-17$	$4.9975e-11$	$9.45e-20$	0.00	0.6448
$1.00e-06$	143252	588529	$7.24e-20$	$4.9940e-13$	$1.51e-21$	0.00	0.6445

Table 3: Example 2: Results on the unit circle with nonconstant V and K, $p = 3$

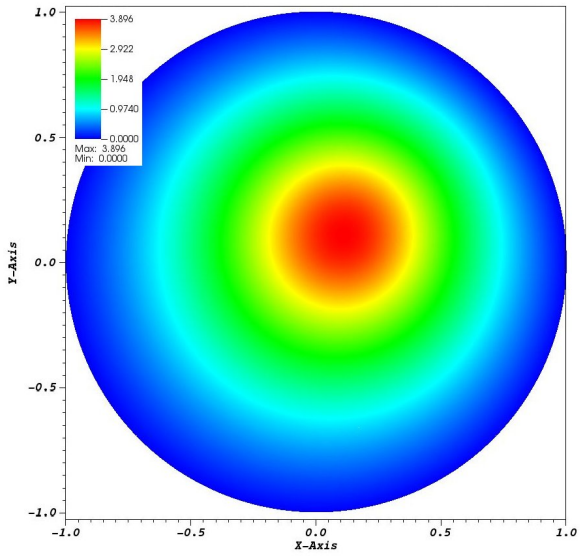

Figure 7: Example 2: Solution u, $\varepsilon = 0.8$

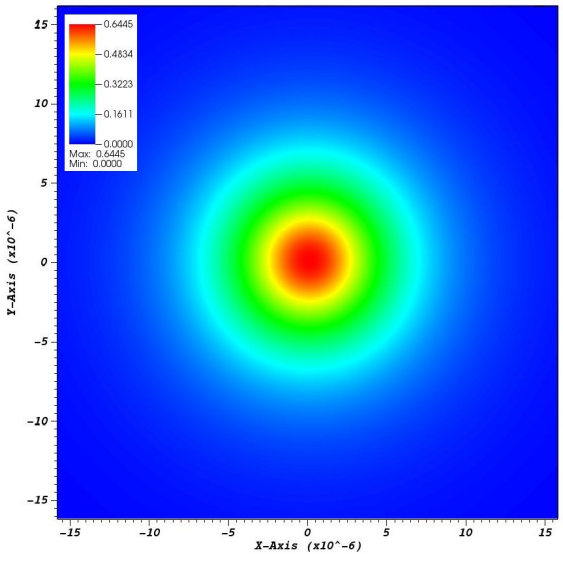

Figure 8: Example 2: Solution u, $\varepsilon = 10^{-6}$

4.3 Example 3: Nonconstant potentials - on a dumbbell-shaped domain

As a third example, we show results on a dumbbell-shaped domain. The left circle of the dumbbell is chosen with radius $r_0 = 0.5$ and center $x_0 = (0,0)^\top$, the right one with $r_1 = 1$ and center $x_1 = (3,0)^\top$. The *bridge* has width 0.5 and we discretize the domain with 6848 cells and 27629 DoF. The potentials V and K are chosen as in the previous example while V has the valley at the center x_0 in the left circle and K has a peak in the center x_1 of right circle. This especially means that the function g from (10) has a global minimum at x_0, $g(x_0) = 0.2$, and another local minimum at x_1, $g(x_1) = 0.76$, see the plot in Figure 9. We start with the initial value w_0 from (29) with $R = 0.5$ and $c = 10$ centered in x_0. The results after 14 mesh refinement cycles are given in Table 4. Similar to the previous example, the asymptotic behavior of the ground-energy decreases proportional to ε^2. Figure 9 shows the solution

ε	# cells	# DoF	$\|A(u_h)\|_2$	$J_\varepsilon(u_h)$	$E(u_h)$	$\min(u_h)$	$\max(u_h)$
$8.00e-01$	223403	912707	$1.15e-12$	$6.9714e+01$	$4.15e-08$	0.00	11.2071
$4.00e-01$	223439	912888	$2.34e-13$	$4.6984e+00$	$2.59e-09$	0.00	5.7720
$2.00e-01$	223145	911711	$5.67e-14$	$3.8183e-01$	$1.69e-10$	0.00	3.2121
$1.00e-01$	221399	900353	$1.96e-14$	$4.6948e-02$	$1.56e-11$	0.00	2.1740
$1.00e-02$	116435	471082	$4.27e-16$	$1.8153e-04$	$2.83e-13$	0.00	1.2954
$1.00e-03$	86534	351135	$1.58e-18$	$1.2556e-06$	$3.00e-15$	0.00	1.9345
$1.00e-04$	117155	491603	$2.94e-11$	$1.6484e-08$	$4.73e-16$	0.00	1.1811
$1.00e-05$	166586	718975	$8.49e-14$	$1.5885e-10$	$5.29e-17$	0.00	1.1521

Table 4: Example 3: Results on the dumbbell-shaped domain with nonconstant V and K, $p = 3$

with a peak in the left circle for $\varepsilon = 10^{-4}$. For smaller values of ε the peak of the solution cannot be visualized in the picture. Also here, solutions do not concentrate exactly at the origin, but *moving* closer to it with decreasing ε. The final mesh with 718975 DoF after 14 refinement cycles for $\varepsilon = 10^{-5}$ is depicted in Figure 10 and zooming into the picture, Figure 11 shows some more *islands* of refined cells formed during the iteration as in the previous example on the unit circle. Here is room for an improvement. Such *islands* can be deleted by local coarsening and this will be part of future work. Nevertheless, the only concentration point of the solution, plotted in Figure 13, is resolved by the refinement strategy and the grid around the peak is plotted in Figure 12. Again, we emphasize the scale of the plots.

Finally, we investigate the behavior of the solution when starting with an initial guess with a peak on the right circle (example 4). For $\varepsilon = 10^{-5}$ the refined mesh is shown in Figure 14. We observe a similar development of refined cells in figures 15 and 16 as on the left circle: there are several *islands* around the local minimum of g, while the solution has exactly one peak shifted a bit from the local minimum of g, see Figure 17. The energy level after 14 mesh refinement cycles and estimated error are

$$J_\varepsilon(u_h) = 4.5068 \cdot 10^{-10}, \quad E(u_h) = 1.57 \cdot 10^{-14}, \quad \|A(u_h)\|_2 = 4.66 \cdot 10^{-13}$$

with 650235 DoF and $\max(u_h) = 1.93$. As mentioned in previous sections, the solution does not exactly concentrates on the local minimum of g, but close to it. Also, the energy level is larger then that corresponding to the solution with peak close to the global minimum of g, what is in agreement with the theoretical results from [WZ97]. While these computed values are very small numbers, the estimated error guarantees at least three digits. This makes it possible to compare the energy levels, a benefit of the error based refinement strategy in combination with the positivity preserving approach.

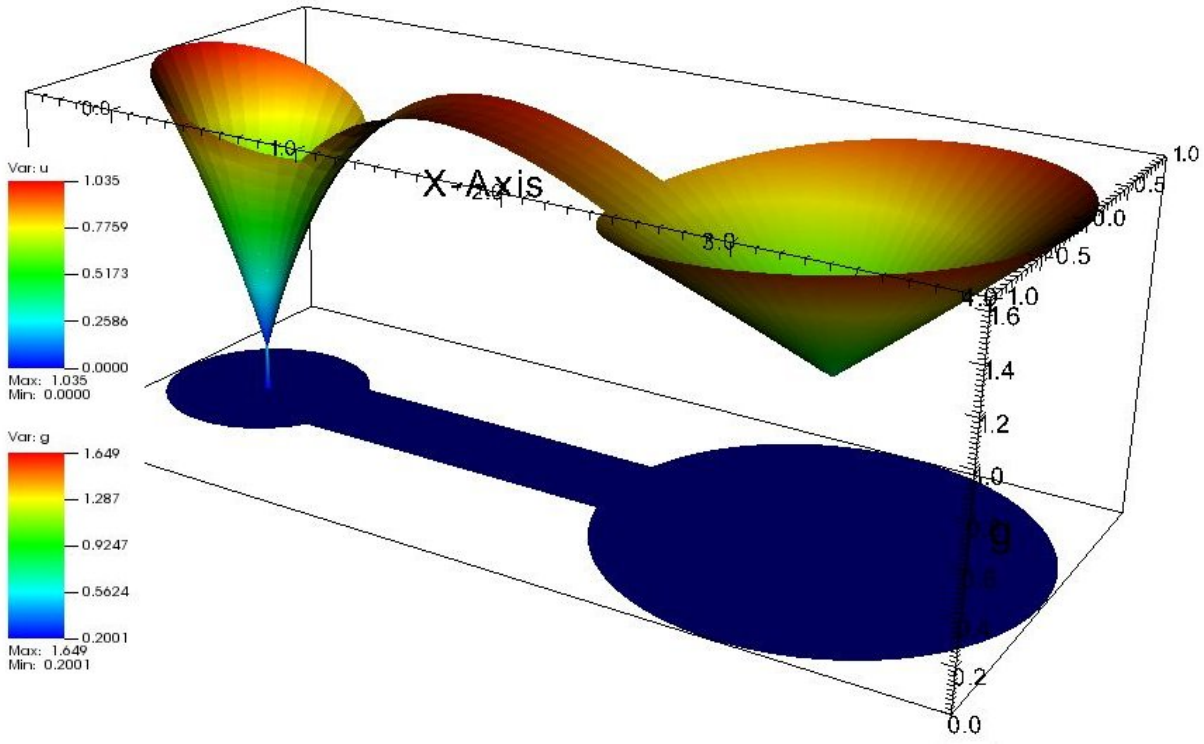

Figure 9: Example 3: Solution u (small peak on the left) and function g, $\varepsilon = 10^{-4}$

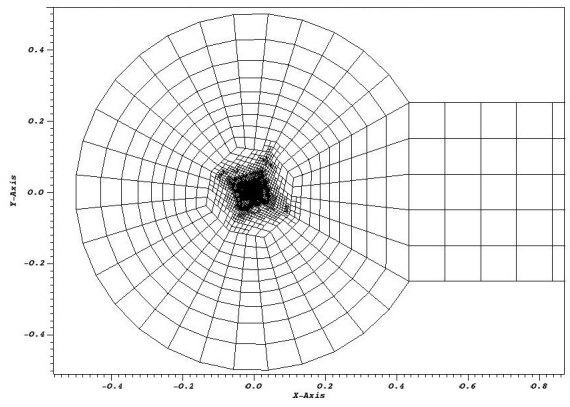

Figure 10: Example 3: Final mesh, 718975 DoF

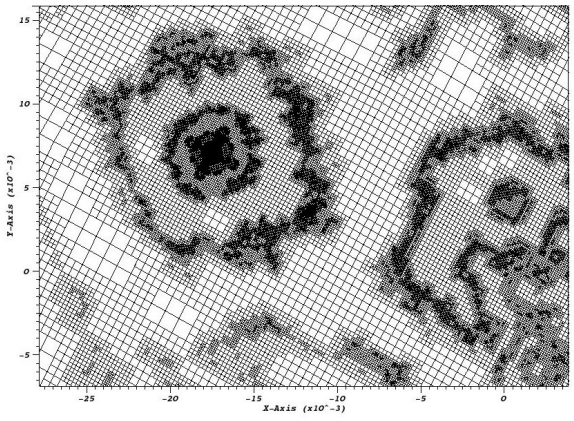

Figure 11: Example 3: Final mesh, zoom 1

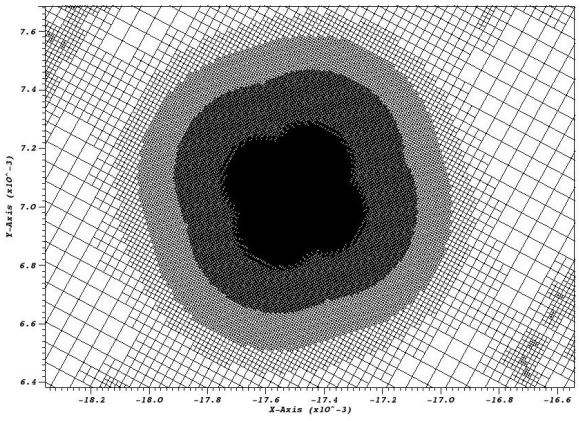

Figure 12: Example 3: Final mesh, zoom 2

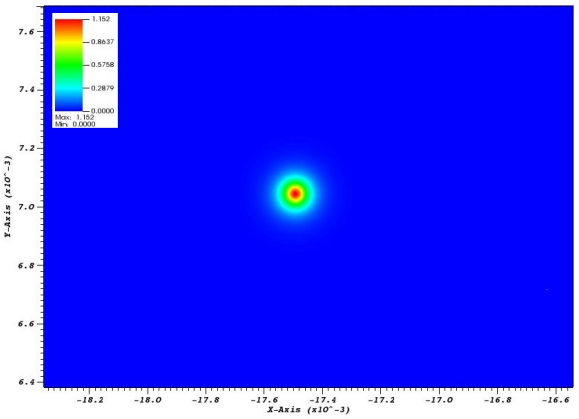

Figure 13: Example 3: Solution u, zoom 2

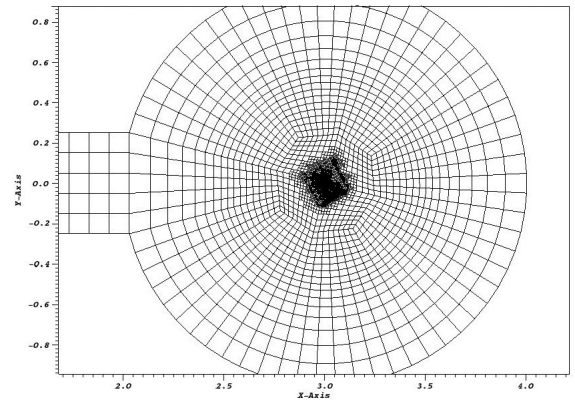

Figure 14: Example 4: Final mesh, 650235 DoF

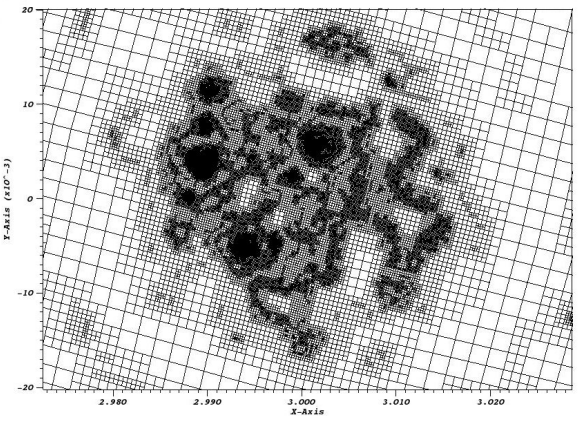

Figure 15: Example 4: Final mesh, zoom 1

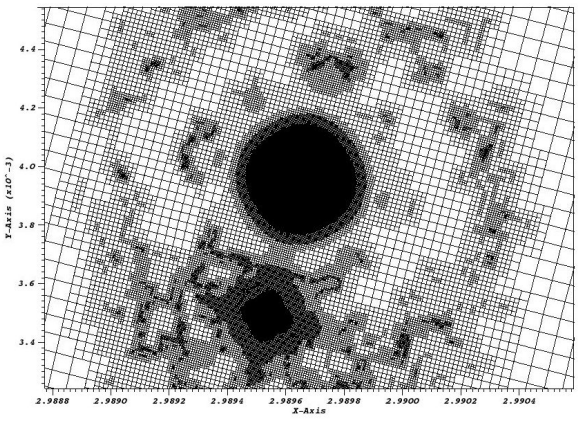

Figure 16: Example 4: Final mesh, zoom 2

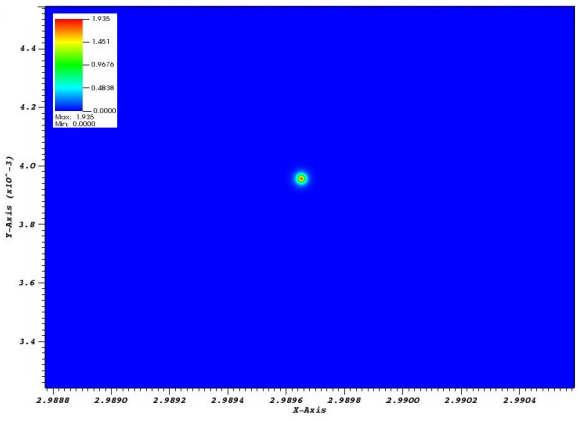

Figure 17: Example 4: Solution u, zoom 2

5. Summary and Outlook

In this paper we have presented a method for computing positive energy solutions of singularly perturbed nonlinear Schrödinger equations. Based on the Mountain Pass geometry, we developed an iteration scheme combining Newton's method with polynomial line searching using finite elements. The key for computing positive solutions of singularly perturbed problems was the combination of the Patankar trick for preserving positivity together with adaptive mesh refinement based on the dual weighted residual approach estimating the error of the energy functional. We have shown numerical results built on the deal.II library for constant and nonconstant potential functions V and K for the unit circle and a dumbbell-shaped domain for parameters down to $\varepsilon = 10^{-6}$, significantly improving schemes known from the literature, which are only applicable for $\varepsilon \geq 10^{-2}$. The results obtained are in absolute agreement with expectations inherent from the theory and clearly show the reliability and robustness of our new method.
There are different directions for future work. The algorithm presented here does not depend on the dimension of the underlying domain and also works in dimension three, but the computational effort will be much higher and requires a more efficient solvers. Also, the combination of our numerical methods with other schemes for obtaining multiple solutions is an interesting aspect. Especially the mesh refinement scheme can be used in linking schemes [DCC99], [CDN01] or with other boundary conditions [XYZ12].

Acknowledgments: The authors A. Ávila and A. Meister gratefully acknowledge financial support by the Deutsche Forschungsgemeinschaft (DFG) through grant ME 1889/4-1 and CONICYT through grant Inst. 117796, CONICYT project No. 653-2011 and Fondecyt No. 1080439. M. Steigemann gratefully acknowledges financial support for hosting a visit at CMCC, Universidad de La Frontera, Temuco, Chile.

References

[AEM+95] M.H. Anderson, J.R. Ensher, M.R. Matthews, C.E. Wieman, and E.A. Cornell, *Observation of Bose-Einstein condensation in a dilute atomic vapor*, Science **269** (1995), no. 5221, 198–201.

[AR73] A. Ambrosetti and P.H. Rabinowitz, *Dual variational methods in critical point theory and applications*, J. Funct. Anal. **14** (1973), 349–381.

[Arm66] L. Armijo, *Minimization of functions having Lipschitz continuous first partial derivatives*, Pacific J. Math. **16** (1966), no. 1, 1–3.

[AZ07] G.L. Alfimov and D.A. Zezyulin, *Nonlinear modes for the Gross-Pitaevskii equation - a demonstrative computation approach*, Nonlinearity **20** (2007), 2075–2092.

[BBHK11] W. Bangerth, C. Burstedde, T. Heister, and M. Kronbichler, *Algorithms and data structures for massively parallel generic adaptive finite element codes*, ACM Trans. Math. Softw. **38** (2011), no. 2, 14:1–14:28.

[BCL06] W. Bao, I-L. Chern, and F.Y. Lim, *Efficient and spectrally accurate numerical methods for computing ground and first excited states in Bose-Einstein condensates*, J. Comput. Phys. **219** (2006), 836–854.

[BCW10] W. Bao, Y. Cai, and H. Wang, *Efficient numerical methods for computing ground states and dynamics of dipolar Bose-Einstein condensates*, J. Comput. Phys. **229** (2010), 7874–7892.

[BD04] W. Bao and Q. Du, *Computing the ground state solution of Bose-Einstein condensates by a normalized gradient flow*, SIAM J. Sci. Comput. **25** (2004), no. 5, 1674–1697.

[BDM03] H. Burchard, E. Deleersnijder, and A. Meister, *A high-order conservative Patankar-type discretization for stiff systems of production-destruction equations*, Appl. Numer. Math. **47** (2003), 1–30.

[BHK07] W. Bangerth, R. Hartmann, and G. Kanschat, *deal.II — a general-purpose object-oriented finite element library*, ACM Trans. Math. Softw. **33** (2007), no. 4, 4.

[BL03] A.D. Bandrauk and H.-Z. Lu, *Numerical methods for molecular time-dependent Schrödinger equations - bridging the perturbative to nonperturbative regime*, Computational Chemistry (C. Le Bris, ed.), Handbook of Numerical Analysis, vol. X, Elsevier, Amsterdam, 2003, pp. 803–832.

[BR03] W. Bangerth and R. Rannacher, *Adaptive finite element methods for differential equations*, Lectures in Mathematics, Birkhäuser Verlag, Basel, Boston, Berlin, 2003.

[BS02] S.C. Brenner and L.R. Scott, *The mathematical theory of finite element methods*, 2nd ed., Texts in Applied Mathematics, vol. 15, Springer, Berlin, New York, 2002.

[BSTH95] C.C. Bradley, C.A. Sackett, J.J. Tollett, and R.G. Hulet, *Evidence of Bose-Einstein condensation in an atomic gas with attractive interactions*, Phys. Rev. Lett. **75** (1995), no. 9, 1687–1691.

[BT03] W. Bao and W. Tang, *Ground-state solution of Bose-Einstein condensate by directly minimizing the energy functional*, J. Comput. Phys. **187** (2003), 230–254.

[CDN01] D.G. Costa, Z. Ding, and J.M. Neuberger, *A numerical investigation of sign-changing solutions to superlinear elliptic equations on symmetric domains*, J. Comp. Appl. Math. **131** (2001), 299–319.

[CEZ02] G. Chen, B.G. Englert, and J. Zhou, *Convergence analysis of an optimal scaling algorithm for semilinear elliptic boundary value problems*, Variational Methods: Open Problems, Recent Progress, and Numerical Algorithms (J.M. Neuberger, ed.), Contemporary Mathematics, vol. 357, AMS, 2002, pp. 69–84.

[CM93] Y.S. Choi and P.J. McKenna, *A mountain pass method for the numerical solution of semilinear elliptic problems*, Nonlinear Anal. TMA **20** (1993), no. 4, 417–437.

[CZN00] G. Chen, J. Zhou, and W.-M. Ni, *Algorithms and visualization for solutions of nonlinear elliptic equations*, Int. J. Bifurcation and Chaos **10** (2000), no. 7, 1565–1612.

[DCC99] Z. Ding, D. Costa, and G. Chen, *A high-linking algorithm for sign-changing solutions of semilinear elliptic equations*, Nonlin. Anal. **38** (1999), 151–172.

[DMA+95] K.B. Davis, M.-O. Mewes, M.R. Andrews, N.J. van Druten, D.S. Durfee, D.M. Kurn, and W. Ketterle, *Bose-Einstein condensation in a gas of sodium atoms*, Phys. Rev. Lett. **75** (1995), no. 22, 3969–3974.

[Gro61] E.P. Gross, *Strucutre of a quantized vortex in Boson systems*, Il Nuovo Cimento **20** (1961), no. 3, 454–477.

[GRPG01] J.J. Garcia-Ripoll and V.M. Pérez-Garcia, *Optimizing Schrödinger functionals using Sobolev gradients: Applications to quantum mechanics and nonlinear optics*, SIAM J. Sci. Comput. **23** (2001), no. 4, 1316–1334.

[Gui96] C. Gui, *Existence of multi-bump solutions for nonlinear Schrödinger equations via variational method*, Comm. Partial Differential Equations **21** (1996), 787–820.

[Kav03] G.M. Kavoulakis, *Bose-Einstein condensation with attractive interactions on a ring*, Phys. Rev. A **67** (2003), 011601.

[Kel99] C.T. Kelley, *Iterative methods for optimization*, SIAM, Philadelphia, 1999.

[KSU03] R. Kanamoto, H. Saito, and M. Ueda, *Quantum phase transition in one-dimensional Bose-Einstein condensates with attractive interactions*, Phys. Rev. A **67** (2003), 013608.

[LZ01] Y. Li and J. Zhou, *A minimax method for finding multiple critical points and its appliactions to semilinear pdes*, SIAM J. SCi. Comput. **23** (2001), no. 3, 840–865.

[Mon11] L. Montoro, *On the numerical computation of mountain pass solutions to some perturbed semi-linear elliptic problems*, SeMA Journal **54** (2011), 65–90.

[NW95] W.-M. Ni and J. Wei, *On the location and profile of spike-layer solutions to singularly perturbed semilinear Dirichlet problems*, Comm. Pure Appl. Math. **48** (1995), no. 7, 731–768.

[Pat80] S.V. Patankar, *Numerical heat transfer and fluid flow*, McGraw-Hill, New York, 1980.

[PGL03] V.M. Perez-Garcia and X.-Y. Liu, *Numerical methods for the simulation of trapped nonlinear Schrödinger systems*, Appl. Math. Comput. **144** (2003), no. 2, 215–235.

[Pit61] L.P. Pitaevskii, *Vortex lines in an imperfect Bose gas*, Soviet Physics JETP **13** (1961), no. 2, 451–454.

[RSS09] N. Raza, S. Sial, and S.S. Siddiqi, *Sobolev gradient approach for the time evolution related to energy minimization of Ginzburg-Landau functionals*, J. Comput. Phys. **228** (2009), 2566–2571.

[TT12] N. Tacheny and C. Troestler, *A mountain pass algorithm with projector*, J. Comput. Appl. Math. **236** (2012), 2025–2036.

[Wan93] X. Wang, *On concentration of positive bound states of nonlinear Schrödinger equations*, Commun. Math. Phys. **153** (1993), 229–244.

[WZ97] X. Wang and B. Zeng, *On concentration of positive bound states of nonlinear Schrödinger equations with competing potential functions*, SIAM j. Math. Anal. **28** (1997), no. 3, 633–655.

[WZ04] Z.-Q. Wang and J. Zhou, *A local Minimax-Newton method for finding multiple saddle points with symmetries*, SIAM J. Numer. Anal. **42** (2004), no. 4, 1745–1759.

[XYZ12] Z. Xie, Y. Yuan, and J. Zhou, *On finding multiple solutions to a singularly perturbed Neumann problem*, SIAM J. Sci. Comput. **34** (2012), no. 1, A395–A420.

[Yan09] J. Yang, *Newton-conjugate-gradient methods for solitary wave computations*, J. Comput. Phys. **228** (2009), 7007–7024.

[YL08] J. Yang and T.I. Lakoba, *Accelerated imaginary-time evolution methods for the computation of solitary waves*, Stud. Appl. Math. **120** (2008), 265–292.

[YZ05] X. Yao and J. Zhou, *A minimax method for finding multiple critical points in Banach spaces and its application to quasi-linear elliptic pde*, SIAM J. Sci. Comput. **26** (2005), no. 5, 1796–1809.

[ZAKPG07] D.A. Zezyulin, G.L. Alfimov, V.V. Konotop, and V.M. Pérez-Garcia, *Control of nonlinear modes by scattering-length management in Bose-Einstein condensates*, Phys. Rev. A **76** (2007), 013621.1–013621.5.

[ZAKPG08] ———, *Stability of excited states of a Bose-Einstein condensate in an anharmonic trap*, Phys. Rev. A **78** (2008), 013606.1–013606.12.